ENVIRONMENTAL RESEARCH
LETTERS

LETTER • OPEN ACCESS

Modelling size distributions of marine plastics under the influence of continuous cascading fragmentation

To cite this article: Mikael L A Kaandorp *et al* 2021 *Environ. Res. Lett.* **16** 054075

IOP Publishing Environ. Res. Lett. 16 (2021) 054075 https://doi.org/10.1088/1748-9326/abe9ea

ENVIRONMENTAL RESEARCH
LETTERS

OPEN ACCESS

RECEIVED
6 November 2020

REVISED
19 February 2021

ACCEPTED FOR PUBLICATION
25 February 2021

PUBLISHED
13 May 2021

LETTER

Modelling size distributions of marine plastics under the influence of continuous cascading fragmentation

Mikael L A Kaandorp*, Henk A Dijkstra and Erik van Sebille

Institute for Marine and Atmospheric research Utrecht, Department of Physics, Utrecht University, Utrecht, The Netherlands
* Author to whom any correspondence should be addressed.

E-mail: m.l.a.kaandorp@uu.nl

Keywords: marine plastics, fragmentation, plastic pollution, size distribution

Supplementary material for this article is available online

Abstract

Field studies in the global ocean have shown that plastic fragments make up the majority of plastic pollution in terms of abundance. It is not well understood how quickly plastics in the marine environmental fragment, however. Here, we study the fragmentation process in the oceanic environment by considering a model which captures continuous fragmentation of particles over time in a cascading fashion. With this cascading fragmentation model we simulate particle size distributions (PSDs), specifying the abundance or mass of particles for different size classes. The fragmentation model is coupled to an environmental box model, simulating the distributions of plastic particles in the ocean, coastal waters, and on the beach. We demonstrate the capabilities of the model by calibrating it to estimated plastic transport in the Mediterranean Sea, and compare the modelled PSDs to available observations in this region. Results are used to illustrate the effect of size-selective processes such as vertical mixing in the water column and resuspension of particles from the beach into coastal waters. The model quantifies the role of fragmentation on the marine plastic mass budget: while fragmentation is a major source of secondary plastic particles in terms of abundance, it seems to have a minor effect on the total mass of particles larger than 0.1 mm. Future comparison to observed PSD data allow us to understand size-selective plastic transport in the environment, and potentially inform us on plastic longevity.

1. Introduction

Studies have shown that fragments make up the majority of marine plastic litter in terms of abundance in the global ocean (Cózar *et al* 2014, Suaria *et al* 2016). The large amount of fragments is evident from particle size distribution (PSD) data, specifying the abundance or mass of particles for different size classes. An overview of PSD data from various studies is given in Kooi and Koelmans (2019); some examples are presented in figure 1. What is commonly observed in PSD data is a power law for larger fragments (>1 mm in figure 1) (Cózar *et al* 2014, 2015, Enders *et al* 2015, Erni-Cassola *et al* 2017), i.e. a straight line on a log-log scale as can be seen in figure 1. Oftentimes, a maximum in the PSD is observed at smaller particle sizes (∼1 mm in figure 1), ending the power law regime. This maximum has been observed to vary, and has been attributed to, for example, the distance to the nearest coast (Isobe *et al* 2014, Pedrotti *et al* 2016).

It is necessary to further investigate the fragmentation process if we want to explain the particular shapes of measured PSD data. Fragmentation of plastics is likely dominant on beaches or inland water bodies such as rivers, where plastics are subjected to UV-radiation, oxidation, and higher temperatures, embrittling the particles, which enhances the breaking down of particles by mechanical abrasion (Andrady 2011, Kalogerakis *et al* 2017, Song *et al* 2017, Efimova *et al* 2018). Fragmentation models have been proposed in e.g. Cózar *et al* (2014), hypothesising that the PSD slope depends on whether particles break down in a three-dimensional fashion (i.e. like a cube), or more in a two-dimensional fashion (like a thin sheet). It has been shown that the polymer type influences how plastic particles fragment (e.g. due to differences in the surface cracks

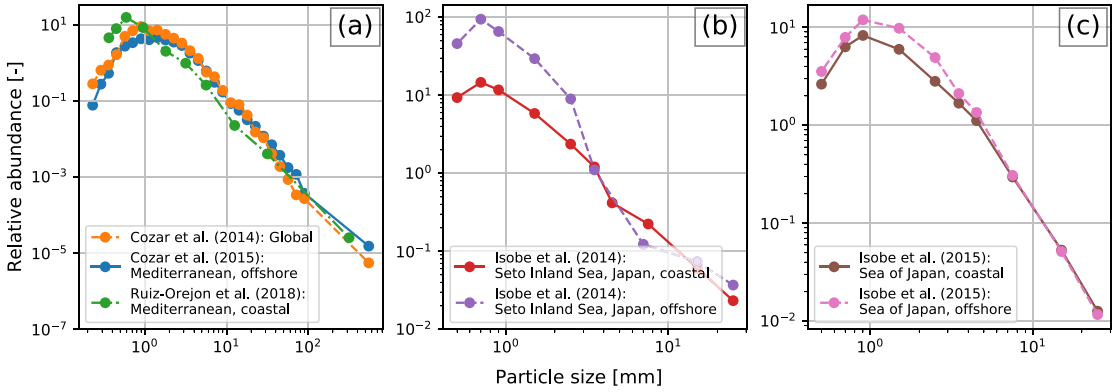

Figure 1. Observed number size distributions. (a) Samples from Cózar *et al* (2014) obtained around the world, and samples from Cózar *et al* (2015) and Ruiz-Orejón *et al* (2018) obtained in the Mediterranean Sea, see the supplementary material (section S3) for locations. (b), (c) Samples from Isobe *et al* (2014, 2015) obtained from the Seto Inland Sea (Japan) and the Sea of Japan. Coastal samples are defined as less than 15 km from the shoreline. All particle size distributions have been normalized relative to the total abundance of large items (>10 mm) to show differences for small particle sizes clearly. Most datasets seem to follow a power law for the larger particle size classes (see figure 7). Coastal samples tend to have relatively few small particles (or: relatively many large particles), and all distributions show a peak in abundance around 1 mm, instead of a monotonic increase with smaller sizes.

(Andrady 2011)), and how quickly plastic particles fragment (Song *et al* 2017), hence directly influencing how PSDs evolve.

While the main driver behind the PSD might be fragmentation, physical processes can have a size-selective influence on plastic particles (van Sebille *et al* 2020). Vertical turbulent mixing, induced by for example the wind, has been shown to mix smaller particles with lower rise velocities to larger depths (Kukulka *et al* 2012, Reisser *et al* 2015, Chor *et al* 2018, Poulain *et al* 2019). This can reduce smaller size fractions in PSDs measured by nets at the ocean surface (typically submerged ±10–50 cm depending on net type, see e.g. Cózar *et al* (2015), Pedrotti *et al* (2016), and Suaria *et al* (2016)). Furthermore, bigger (more buoyant) particles likely experience more influence from Stokes drift, given its limited depth of influence (Breivik *et al* 2016, Bremer and Breivik 2017). Model studies have indicated that Stokes drift tends to push plastic particles towards coastal areas (Iwasaki *et al* 2017, Delandmeter and van Sebille 2019, Onink *et al* 2019). In Isobe *et al* (2014) it was observed that for coastal seas near Japan, overabundances of larger plastic particles were found close to the coast versus more offshore, see figure 1(b). Coastal processes, such as beaching and resuspension, can be size-selective. In Hinata *et al* (2017), residence times of particles on beaches in Japan were estimated using tagged litter. Higher particle rise velocities in the water were related to longer residence times, as these particles are more likely to be pushed to the backshore by wave swash. This could mean that larger objects remain longer on beaches, and hence experience more weathering (Hinata *et al* 2020). Finally, PSDs could be influenced by size selective sinking, induced by for example biofouling (Ryan 2015). Biofouling models predict that smaller particles, which have a larger surface to volume ratio, tend to sink more quickly (Kooi *et al* 2017). This has been observed in experimental studies as well (Fazey and Ryan 2016).

Previous studies, such as the ones by Koelmans *et al* (2017) and Lebreton *et al* (2019), have tried to quantify marine plastic mass budget using conceptual models. In both of these works, fragmentation is purely defined as a rate, breaking down a mass percentage of a macroplastics category into a microplastics category over time. How, and how quickly plastics fragment is still a very uncertain factor however.

In this work, we consider a fragmentation model based on fractal theory (Turcotte 1986, Charalambous 2015), modelling a large range of different size classes. A benefit of modelling a range of size classes is that we can calibrate the model to experimental fragmentation studies such as the one by Song *et al* (2017), where different polymers were subjected to laboratory conditions simulating weathering in the marine environment. By modelling a range of size classes, we can furthermore compare model output to measured PSDs in the environment, such as the ones presented in figure 1.

We couple our fragmentation model to an idealized box model where the marine environment is split into three different compartments, similar to Lebreton *et al* (2019): the beach, coastal water, and open ocean. By considering a range of size classes, we can study size-dependent processes in the marine environment mentioned earlier and their influence on the fragmentation process and resulting PSDs. Finally, our model allows quantification of PSDs both in terms of the amount of particles in each size class, and the particle mass in each size class. We will make a distinction between the two, and call them the number (i.e. abundance) size distribution (NSD), and the mass size distribution (MSD). We will use the term PSD when talking about size distributions in general

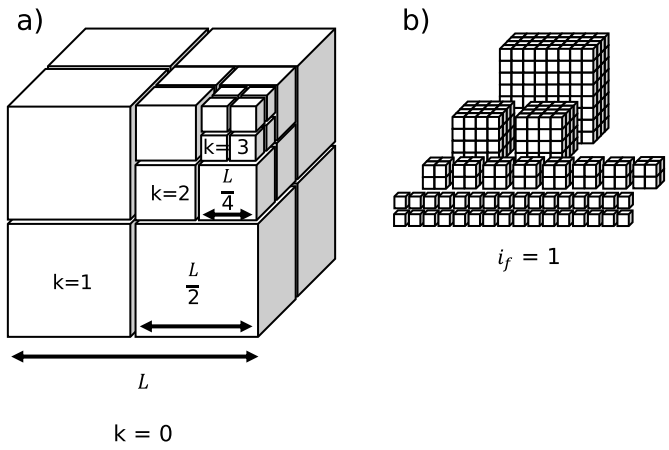

Figure 2. (a) Illustration of a parent cube (size class $k = 0$), consisting of successively smaller cubes, based on Turcotte (1986). Only three iterations until size class $k = 3$ are shown here, the size class can increase indefinitely. (b) Illustration of the cascading fragmentation model with $p = 0.5$ and after one fragmentation event i_f, based on Turcotte (1986) and Charalambous (2015).

(i.e. either NSD or MSD). We will show that with these MSD data, our model can contribute to obtain a better understanding of the plastic mass budget. Similar to the models in Koelmans *et al* (2017) and Lebreton *et al* (2019), the idealized model presented here allows us to efficiently test hypotheses regarding fragmentation, sources, sinks, and transport of marine plastics. We will demonstrate this by applying the model to different marine plastic scenarios in the Mediterranean Sea. The goal is to have an analysis which is consistent with current experimental data of the fragmentation process, observational data in terms of plastic concentrations and plastic PSD data, and current knowledge on marine plastic sources, sinks, and transport.

2. Methodology

2.1. The cascading fragmentation model

The fragmentation model discussed here is based on simple fractal geometries. We define the spatial dimension as D_N. When $D_N = 3$, we start with a cube with a size of $L \times L \times L$ which we call the parent object, see figure 2(a). This cube can be split in eight equally-sized cubes, which can each be recursively split again. The size class of the parent object is defined as $k = 0$, the size class of the cubes with length $L/2$ is defined as $k = 1$, and so on. When $D_N = 2$, the starting object is a sheet instead of a cube, which can be split in four smaller sheets each time the size class increases.

Cózar *et al* (2014) presented a fragmentation model where objects are broken down into a set of smaller (equally sized) fragments in a series of successive fragmentation events. This fragmentation model was used to explain why measured PSDs often resemble power laws, i.e. functions of the form:

$$n(l) = Cl^{-\alpha}, \tag{1}$$

where n is the abundance, l is the particle size, α is the power law slope, and C is a constant. However, this fragmentation model requires a constant input of new parent objects to achieve a power law, while laboratory experiments have shown that power laws in the PSD also appear after fragmenting a single input of parent objects (Song *et al* 2017).

The fragmentation model used here builds upon the work of Turcotte (1986), where it was noted that scale-invariance of the fragmentation process, whether it be caused by weathering, explosions, or impacts, leads to such a power law. The idea behind the model of Turcotte (1986) can be illustrated using figure 2(b). Following one fragmentation event i_f, a certain fraction p of the original cube (size class $k = 0$) splits off. For example, if $p = 0.5$, this results in 4 fragments of $k = 1$ splitting off, leaving 0.5 object in size class $k = 0$. This process is assumed to be the same on all length scales: a fraction p will split off from the fragments in size class $k = 1$ as well: 16 fragments of size class $k = 2$ are created, and $4 \times 0.5 = 2$ fragments are left in size class $k = 1$. This process is repeated indefinitely.

Bird *et al* (2009) and Gregory *et al* (2012) extended this model by including a temporal component, with each fragment breaking down further as i_f progresses. Charalambous (2015) showed that repeatedly breaking down fragments over discrete steps of i_f is a sequence of independent and identical Bernoulli trials with a chance of success p, yielding a negative binomial distribution. This is rewritten in terms of a continuous fragmentation index f (instead of the discrete i_f), yielding a probability density function giving the mass m in size class k at fragmentation index f as:

$$m(k; f, p) = \frac{\Gamma(k+f)}{\Gamma(k+1)\Gamma(f)} p^k (1-p)^f, \tag{2}$$

where Γ is the gamma function. We will call this model, introduced in Charalambous (2015), the

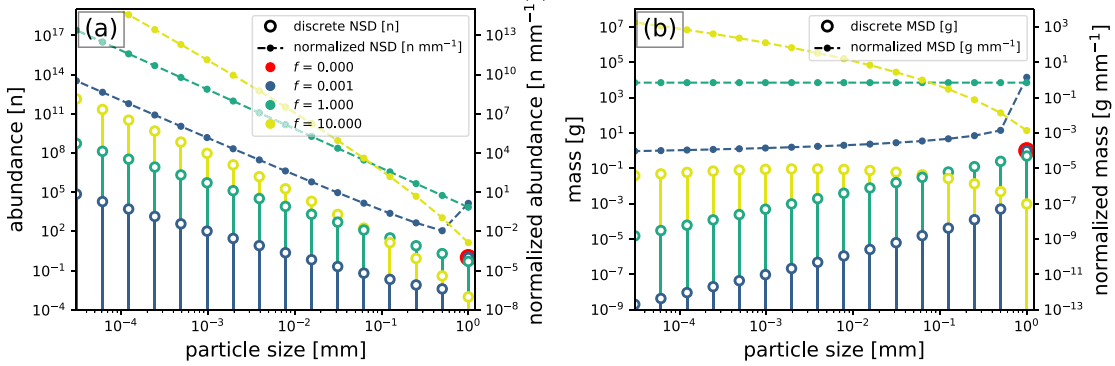

Figure 3. Particle size distributions from the cascading fragmentation model, using $p = 0.5$. Distributions for different fragmentation indices f are shown. (a) The discrete NSD (left y-axis) and the NSD normalized with respect to the particle size (right y-axis). (b) The discrete MSD (left y-axis) and the normalized MSD (right y-axis).

cascading fragmentation model. We assume that f is directly proportional to time in the environment, and will review this assumption in the discussion.

The amount of fragments in a given size class is estimated by multiplying the mass with $2^{D_N k}$, a factor determining how many fragments of size class k fit inside the parent object:

$$n(k,f,p) = 2^{D_N k}\, m(k;f,p). \tag{3}$$

We use $D_N = 3$ as the baseline. However, this factor is $D_N = 2$ for purely flat objects like plastic sheets and $D_N = 1$ for fibres or lines. As real-world samples contain a combination of these objects, the value for D_N in the environment can be a non-integer between 1 and 3. The value of D_N is only influenced by the shape of the objects. The material properties (e.g. polymer type) only affect the value of p and how quickly f progresses in time.

Figure 3(a) shows the NSD resulting from the cascading fragmentation model at various fragmentation indices f. We start with one cube with a length L of 1 mm at $f = 0$. The continuous description in (3) allows us to model the amount of fragments at a very small fragmentation index of $f = 0.001$. There are few larger fragments ($>10^{-2}$ mm) per parent object at this stage. At $f = 1$ we have exactly a power law in the NSD, equivalent to the model by Turcotte (1986) which only considers a single discrete fragmentation event i_f. A fractal dimension D_f of the object formed by all fractions can be defined, relating to D_N and p by:

$$D_f = \log_2\left(2^{D_N} p\right). \tag{4}$$

The NSD power law slope at $f = 1$ is given by this fractal dimension.

Fragments can be broken down further, eventually resulting in the NSD shown for $f = 10$. This is not a power law anymore, and the slope of this curve has increased significantly, with relatively many particles in the small size classes. The NSD (units: n) can be normalized, by dividing the amount of fragments by the size class bin width (units: n mm^{-1}). These normalized NSDs are presented by the dashed lines. Because of the log-scale on the x-axis, the distance between the given particle sizes increases by a constant factor. This increases the magnitude of the normalized NSD slopes by 1 compared to the discrete NSD. The slope of these normalized NSDs is not dependent on the size class bins used for the measurements, allowing for comparison between different studies.

Figure 3(b) shows the same analysis in terms of mass, i.e. the MSD, starting with one cube of 1 g and 1 mm^3. As fragmentation progresses, mass shifts from the large fragments towards smaller fragments. At $f = 1$ we have a power law: the difference in the slope between the NSD and MSD is 3, resulting from the $2^{D_N k}$ term in (3), with $D_N = 3$.

2.2. Environmental box model

With the cascading fragmentation model we can now simulate PSDs over time. Different particle sizes will undergo different types of forcing and transport in the environment. The combination of fragmentation and size-selective transport is investigated using a box model, presented in figure 4. The boxes in this model represent three different environmental regions: the beach, coastal waters, and open ocean.

Particles can move between the different environments, defined by a set of transition probabilities (P): particles can move to a different environmental box (the arrows on the right in figure 4), remain in the current box (recurring arrows on the left), or vanish from the system (i.e. a sink, arrows on the left). Subscripts in figure 4 denote ocean, coast, beach, or sink (O, C, B, and S respectively).

Besides different environmental regions, we have different particle size classes. For a given size class, certain mass fractions will move to smaller size classes under the influence of fragmentation. These fractions are estimated by evaluating (2) for the given time step of the box model. Similarly, (3) is evaluated to determine the abundance of fragments moving to

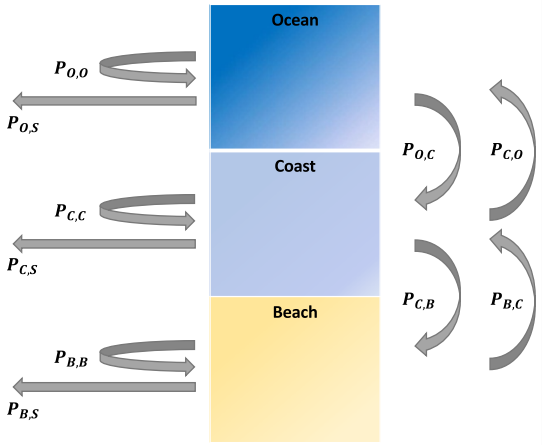

Figure 4. Environmental box model used to simulate particle size distributions in the marine environment. Particles move between and within the ocean, coast, and beach boxes, and for each box there is a probability of being removed from the system.

smaller size classes. Fragmentation is assumed to only happen on the beach, where degradation is expected to be much more effective than in the sea (Andrady *et al* 1993, Andrady 2011).

Each environmental box contains a range of different particle size classes. The combination of environmental transition probabilities and fragmentation is modelled using a transition matrix. For example, taking 15 different size classes and 3 environmental compartments leads to a transition matrix of size 45×45. Further details are given in the supplementary material (section S2), available online at stacks.iop.org/ERL/16/054075/mmedia.

2.3. Applying the box model to the Mediterranean Sea

We will demonstrate the capabilities of the environmental box model using a set-up based on the Mediterranean Sea. Environmental transition probabilities are derived from the literature on plastic transport in the Mediterranean Sea as much as possible. The different parameters, the studies on which they are based, and the areas of these studies are shown in table 1.

2.3.1. Transport in the marine environment

A Lagrangian simulation of floating plastic in the Mediterranean Sea (Kaandorp *et al* 2020) is used to determine transition probabilities within and between the ocean and coast ($P_{O,O}$, $P_{O,C}$, $P_{C,C}$, and $P_{C,O}$). The coast is defined as the ocean within 15 km of the coastline.

Previous model studies have indicated that Stokes drift is able to push floating particles towards the coast, e.g. in the North Atlantic (Onink *et al* 2019), the North Sea (Delandmeter and van Sebille 2019), and in the Sea of Japan (Iwasaki *et al* 2017). It has been hypothesised that this leads to near-shore trapping of larger plastic particles, as more buoyant particles would tend to reside closer to the water surface, where they experience more influence from the Stokes drift (Isobe *et al* 2014, Iwasaki *et al* 2017).

We investigate the effect of this near-shore trapping of larger plastic particles and its influence on fragmentation. First, we calculate the transition probabilities assuming all particle sizes reside at the ocean surface, where they experience the maximum Stokes drift (corresponding to the transition probabilities between the ocean and coast in table 1). We then compute how differently sized particles are vertically distributed in the water column, and how this influences the lateral transport induced by Stokes drift. The approach from Poulain *et al* (2019) is used to estimate particle rise velocities w_b for different particle sizes, see the supplementary material (section S3) for further details. From these rise velocities we calculate the median particle depth, using the particle density profiles from Kukulka *et al* (2012). The Stokes drift is estimated at this depth, assuming a Stokes profile based on the Phillips wave spectrum (Breivik *et al* 2016). For this Stokes drift, the transition probabilities are calculated using Lagrangian model simulations (Kaandorp *et al* 2020) with different Stokes drift factors. In the end, this gives us different transition probabilities ($P_{O,O}$, $P_{O,C}$, $P_{C,C}$, and $P_{C,O}$) for each particle size. More information and resulting transition probability values are given in the supplementary material (sections S1 and S3).

Using the same approach as in Kaandorp *et al* (2020), we estimate $P_{C,B}$ by analysing drifter buoy data: from a set of 1682 drifters in the Mediterranean (Menna *et al* 2017), we calculate how much time these drifters spend near the coast before beaching. For drifter buoys within 15 km of the coastline, the beaching rate is estimated to be about 6.7×10^{-3} d^{-1} (corresponding to an e-folding time-scale τ_{CB} of 149 days). In Kaandorp *et al* (2020) it was estimated that τ_{CB} for plastic particles is about three times lower than that for drifter buoys. We will therefore use $\tau_{CB} = 50$ days as the baseline estimate here.

We use data from Hinata *et al* (2017) to estimate residence times τ_{BC} of plastic particles on beaches, to obtain $P_{B,C}$ and $P_{B,B}$. This study was conducted on a beach in Japan, no information could be found for the Mediterranean Sea specifically. We therefore assume that the Japanese setting is representative of the Mediterranean too: a sensitivity study for τ_{BC} is presented in the supplementary material (S1). As a baseline estimate we use $\tau_{BC} = 211$ d, reported for small plastic floats (corresponding to the baseline $P_{B,C}$ in table 1). We will then investigate the effect of size-selective resuspension, for which the empirical relation from Hinata *et al* (2017) is used, i.e.

$$\tau_{BC}(w_b) = 2.6 \times 10^2 \, w_b + 7.1, \qquad (5)$$

where τ_{BC} is given in days, and w_b in m s^{-1}.

Table 1. Environmental box model parameters and fragmentation parameters, references used to estimate the parameter values, the respective study areas, and the estimated baseline parameter values.

Parameter	Reference study or data	Reference study area	Baseline parameter value
$P_{O,O}$	Kaandorp *et al* (2020)	Mediterranean	7.2×10^{-1} week^{-1}
$P_{O,C}$	Kaandorp *et al* (2020)	Mediterranean	2.7×10^{-1} week^{-1}
$P_{C,O}$	Kaandorp *et al* (2020)	Mediterranean	3.4×10^{-2} week^{-1}
$P_{C,C}$	Kaandorp *et al* (2020)	Mediterranean	8.3×10^{-1} week^{-1}
$P_{C,B}$	Menna *et al* (2017), Kaandorp *et al* (2020)	Mediterranean	1.3×10^{-1} week^{-1}
$P_{B,C}$	Hinata *et al* (2017)	Japan	3.2×10^{-2} week^{-1}
$P_{B,B}$	Hinata *et al* (2017)	Japan	9.6×10^{-1} week^{-1}
P_S	Cózar *et al* (2015), Kaandorp *et al* (2020)	Mediterranean	5.1×10^{-3} week^{-1}
Input	Kaandorp *et al* (2020)	Mediterranean	2500 t year^{-1}
p	Song *et al* (2017)	South Korea	0.4
λ	Song *et al* (2017)	South Korea	$1.8 \times 10^{-2} f$ week^{-1}

The box model also requires transition probabilities for removal of particles: $P_{O,S}$, $P_{C,S}$, $P_{B,S}$. We assume these are the same in all compartments, denoted by P_S. A given value for P_S yields a certain amount of steady-state mass in the system. We take the estimated input of waste into the Mediterranean from Kaandorp *et al* (2020) (2500 metric tonnes for the year 2015), and the estimated total floating mass from Cózar *et al* (2015) (2000 metric tonnes). The value for P_S is iterated until this mass balance is satisfied, see the supplementary material (section S2) for more information.

Finally, we need to specify the plastic input into the marine environment in terms of location and shape. We assume that new plastic objects are introduced on the beach. This assumption does not affect results significantly, see the supplementary material (S1). We use an initial length of 200 mm based on typical dimensions of municipal plastic waste in the Netherlands (Jansen *et al* (2015), see the supplementary material section S4), assuming that plastic product dimensions are similar to those used around the Mediterranean Sea. We use $D_N = 3$ as the baseline, i.e. cubical-shaped objects. The model time step is set to 1 week.

2.3.2. Fragmentation parameters

We use data from Song *et al* (2017) to estimate the fragmentation parameter p, and to estimate the fragmentation rate λ specifying how much f increases per unit time.

In Song *et al* (2017), plastic pellets were subjected to different levels of UV exposure and to 2 months of mechanical abrasion with sand, simulating a beach environment. The data for polyethylene (PE) and polypropylene (PP) pellets (26 and 19 mm^3 respectively) are used, as these are the most abundant polymers in the Mediterranean surface waters (PE: 52%–76%, PP: 7%–16% (Pedrotti *et al* 2016, Suaria *et al* 2016)).

We assume a single p value per material, and $D_N = 3$. The fragmentation index f is allowed to vary between the different levels of UV exposure when fitting the data. By fixing p and varying f, we get a robust estimate for the unknown parameter p for which we need a plausible value in the box model. We can expect that f is larger for particles subjected to longer periods of UV exposure, since embrittlement will make it easier for the mechanical abrasion to wear down the particles.

Resulting NSD fits using weighted least squares are presented in figure 5, top row, fitted values for f are presented in the legend. For PE particles, the best fit results in $p = 0.39$, for PP particles $p = 0.45$. The experimental data are still at the early stage of fragmentation ($f < 1$), with few fragments per parent pellet, except for small fragment sizes.

There is a good fit for the PE data, with almost all simulations within the data error bars (one relative standard deviation). For PP there is a good fit for 0, 2 and 6 months of UV exposure. At 12 months of UV exposure there is more mismatch for the smallest size class (0.05–0.10 mm). This is also the only case where the estimated f is lower than for the previous level of UV exposure.

The bottom row of figure 5 compares the estimated volume fractions of the parent pellets and the fragments. Generally, the modelled volume fraction of the parent pellet is estimated reasonably well, although there is some overprediction for PE with 12 months of UV exposure. The modelled fragment volumes are higher than the ones estimated in Song *et al* (2017). A possible explanation is that some of the larger fragments could have been missed in the experimental setting since there are very few of these per parent object (e.g. tenths or hundredths). One can see in figure 3 that at an early stage of fragmentation ($f < 1$), the larger fragments contribute little to the total abundance of fragments (figure 3(a)), but a lot to the total volume or mass of fragments (figure 3(b)). In the experimental setting ten parent objects per sample were used, and fragments were counted under magnification on 0.7%–5% of the filter paper area. The larger fragments could therefore have been missed, or even have a low probability of actually existing.

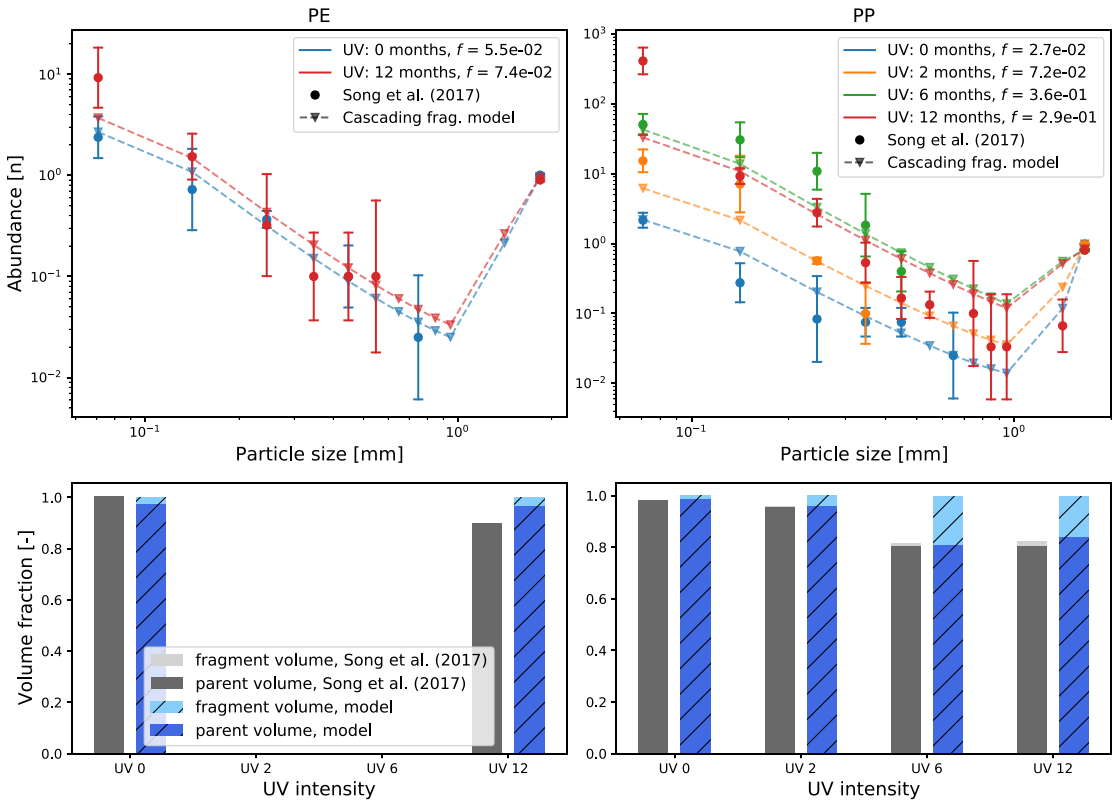

Figure 5. Calibration of the cascading fragmentation model with experimental data from Song *et al* (2017). The experimental data is shown using the circles, including error bars representing the relative error (one time the sample standard deviation). The fragmentation model results are shown using the triangles and dashed lines.

Following this analysis, we set the baseline value of p in the box model to 0.4, within the range of the fitted p for PE and PP. A fragmentation rate λ needs to be chosen, specifying how much f increases per unit time. We assume that λ is a constant, meaning that the amount of fragmentation f is directly proportional to the time that particles spend on the beach.

In Song *et al* (2017) 12 months of laboratory UV exposure were roughly related to 4.2 years of environmental exposure, representing beach conditions in South Korea. Regarding UV exposure, these conditions are quite similar to the Mediterranean (Herman *et al* 1999). Taking our estimated fragmentation indices for PE and PP results in fragmentation rates λ of $1.8 \times 10^{-2}\, f\, \mathrm{y}^{-1}$ to $6.9 \times 10^{-2}\, f\, \mathrm{y}^{-1}$. The value for PE is used as the baseline here, given it is the most common polymer in the Mediterranean surface water (Pedrotti *et al* 2016).

In Song *et al* (2017) low-density polyethylene pellets are used: future studies are necessary to analyse how the results change for high-density polyethylene. We acknowledge that the fragmentation rate λ is still very uncertain, and more experimental research is necessary to verify whether the assumption that f varies linearly in time is a good approximation.

3. Results

3.1. Modelled environmental particle size distributions

Now that we have estimates for transition probabilities in the box model and estimates for the fragmentation parameters, we will simulate PSDs using a scenario based on the Mediterranean Sea. We will quantify the power law slope α of the results by numerically maximizing the log-likelihood ℓ of the data (Virkar and Clauset 2014):

$$\ell = n(\alpha - 1)\ln b_{\min} + \sum_{i=\min}^{k} n_i \ln\left(b_i^{(1-\alpha)} - b_{i+1}^{(1-\alpha)}\right), \tag{6}$$

where b are the bin boundaries used to discretize the data, containing n_i samples in the bin with index i, and $n = \sum n_i$. In some cases, not the entire particle size range adheres to a power law. The lower bound of the power law domain is estimated by minimizing the Kolmogorov–Smirnov statistic between the modelled NSD and the theoretical power law NSD (Virkar and Clauset 2014).

NSDs resulting from the box model are shown in figure 6, corresponding MSDs and a table with parameter settings can be found in the supplementary

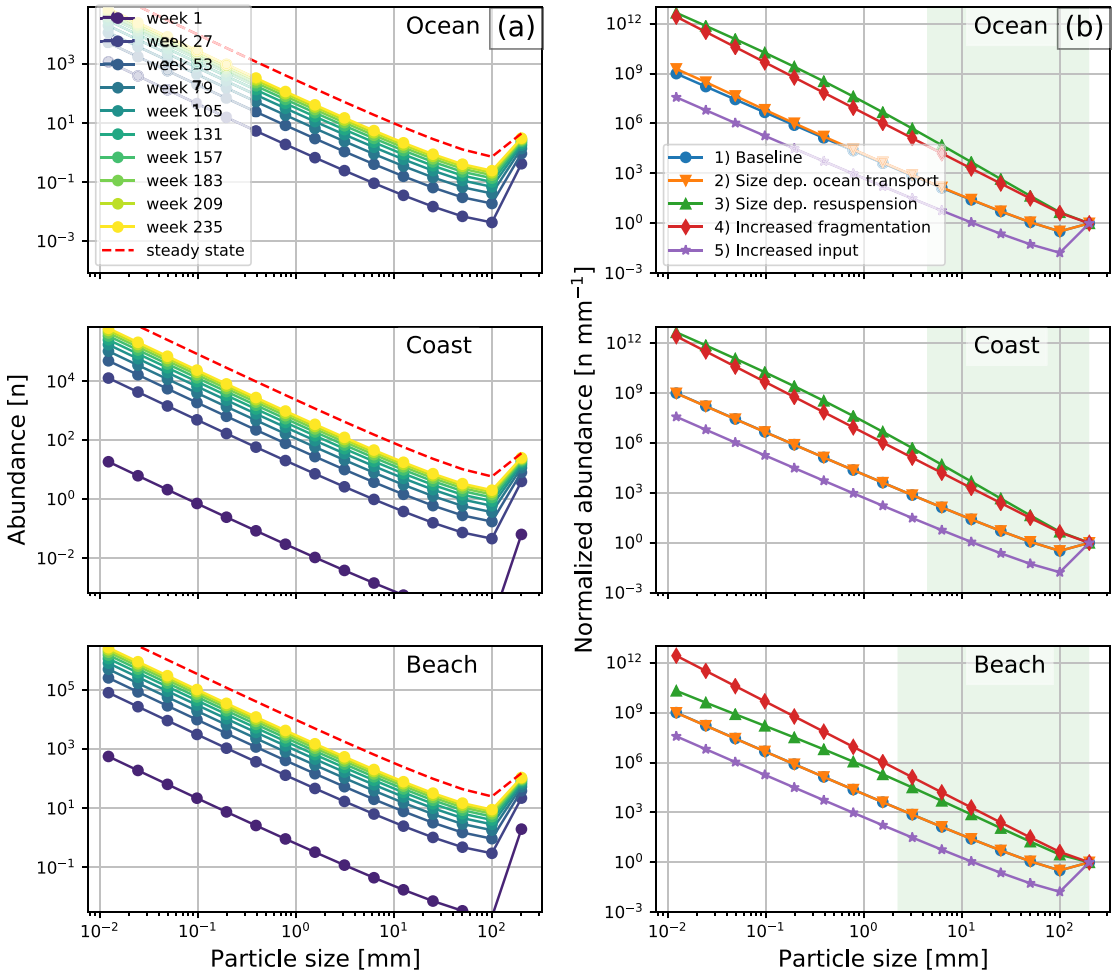

Figure 6. Modelling NSDs using the environmental box model. Column a: transient response to a constant input of particles into the model (baseline scenario). Column b: steady state normalized NSDs for different environmental scenarios, normalized to the amount of parent particles (200 mm). The approach from Virkar and Clauset (2014) is used to determine the power law size range: for most scenarios, α is calculated over the entire size range except for scenario 3, which is shown using the green shading.

material (section S1). Fragmentation is expected to increase the fraction of small particles, increasing α over time (see figure 3). However, environmental sinks limit the magnitude of α: assuming a constant removal rate of plastic particles, smaller fragments, which tend to be older, have a higher probability of being removed from the environment. This combination of fragmentation and environmental sinks eventually leads to an equilibrium, or statistical steady state. This is illustrated in figure 6(a) using the box model with the baseline parameters described in section 2.2. As time progresses, the relative proportion of fragments to parent objects increases. In this scenario, it takes on the order of years for the NSD to resemble the steady state (red dashed line). The magnitude of the environmental sinks is high enough to avoid long persistence of fragmented particles: there are still relatively many parent objects, and $\alpha = 2.57$ is still below the value derived from the fractal dimension of $\alpha = 2.67$ from (4).

Steady state NSDs for different scenarios are presented in figure 6(b). Results for the baseline parameters (blue lines) almost overlap with the results where size-selective lateral transport is added to the box model, induced by vertical mixing and Stokes drift (orange lines). In the baseline scenario $\alpha = 2.57$ for all three NSDs. When adding size-selective ocean transport, larger particles tend to move more frequently from the ocean to the coast. This results in slightly more small particles in the ocean box, increasing the power law slope here to $\alpha = 2.73$. Adding size-selective resuspension of particles (Hinata *et al* 2017) has a strong effect (green lines). Bigger objects have longer residence times on the beach, and therefore undergo more fragmentation. This produces a large number of smaller fragments with shorter residence times, which therefore move more rapidly to the coastal and ocean cells. This near-shore trapping of larger plastic objects was already hypothesized in e.g. Isobe *et al* (2014). The empirical resuspension relation (5) causes the model to deviate from a power law, the domain over which α is calculated is shaded in green in figure 6. The model yields $\alpha = 2.69$ on the beach, which is lower than in the coastal and ocean cells (both $\alpha = 3.37$). A scenario where the fragmentation rate is based on PP

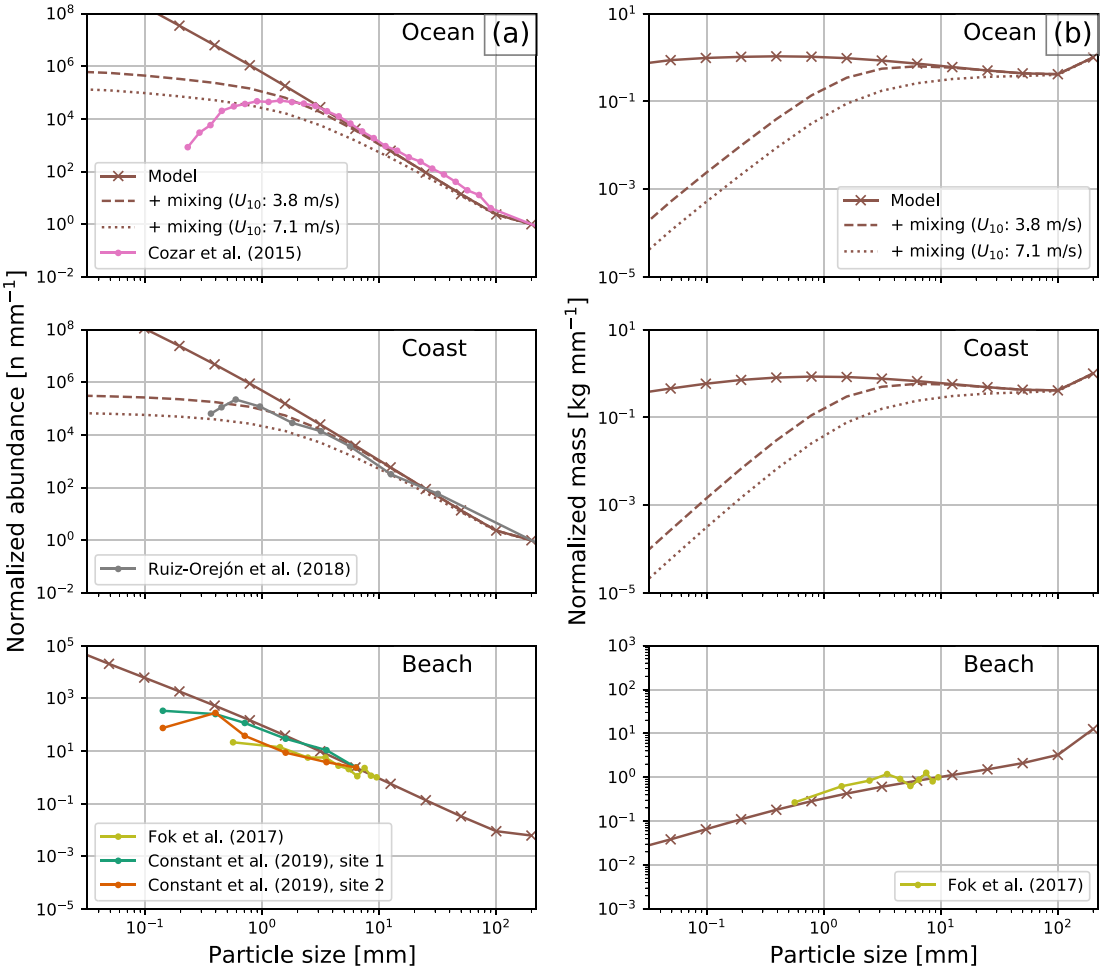

Figure 7. Comparison of modelled and measured PSDs, along with effects of vertical mixing induced by turbulence on measured particle sizes. PSDs are normalized to the maximum observed size class, if no measurements are available to the maximum modelled size class. Column a: comparison of NSDs. Column b: comparison of MSDs.

instead of PE is presented (red lines). Fragmentation breaks down the particles more quickly: a monotonic relation between particle size and abundance is observed, with $\alpha = 3.03$. Finally, a scenario is presented (purple lines) where the input of plastic waste into the Mediterranean is 100 000 tonnes per year (Jambeck *et al* 2015, Liubartseva *et al* 2018), instead of the aforementioned 2500 tonnes per year (Kaandorp *et al* 2020). The magnitude of the sinks needs to be much larger now to attain a mass balance based on 2000 tonnes of floating plastics (Cózar *et al* 2015). Fragmentation has little time to break down the particles, resulting in relatively few fragments per parent object.

In figure 7, we compare PSDs resulting from the box model with observed ones in the Mediterranean Sea. In the model results we include both size dependent ocean transport and resuspension. Fragmentation parameters are set to $\lambda = 2 \times 10^{-4}$ f week^{-1}, and $D_N = 2.5$, resulting in good agreement with the observed PSDs. The effect of vertical turbulent mixing of fragments using the model from Poulain *et al* (2019) is shown as well (calm, $U_{10} \approx 4$ m s^{-1}, and above average, $U_{10} \approx 7$ m s^{-1} conditions based on the 30% and 70% quantile of Mediterranean sea weather conditions (Hersbach *et al* 2020), see supplementary material section S3), assuming a submerged net depth of 25 cm (similar to e.g. Cózar *et al* (2015)).

Figure 7(a) presents the resulting NSDs. We compare model results in the ocean cell with measurements by Cózar *et al* (2015), and results in the coastal cell with measurements by Ruiz-Orejón *et al* (2018), as these were mainly obtained further away from the coast or close to the coast respectively (see the supplementary material: section S3, figure S8). Under calm wind and wave conditions there is good agreement between the modelled and observed NSDs. Vertical mixing causes the modelled NSDs to deviate from the power law around <3 mm, similar to the measured NSDs. Many of the smaller fragments are expected to be mixed below the net depth, resulting in measuring only a fraction of small fragments. This, combined with a size detection limit effect where elongated particles escape from meshes smaller than their maximum length (Enders *et al* 2015, Abeynayaka *et al* 2020, Tokai *et al* 2021), could explain a part of the underabundance of sub-millimetre fragments in observations. Measurement campaigns with much smaller size-detection limits than the standard

neuston nets (see e.g. Enders *et al* (2015) or Kooi and Koelmans (2019)) show increasing abundances for sub-millimetre fragments. It is therefore unlikely that the underabundance of sub-millimetre fragments is explained by an increased loss of these particles, suggested in some studies (Cózar *et al* 2014, Pedrotti *et al* 2016).

Including vertical mixing has a strong effect on the estimated power law slope α. An overview of the estimated α and the power law size range for figure 7(a) is given in the supplementary material, section S1. In the ocean cell, $\alpha = 2.73$ without vertical mixing, and decreases to $\alpha = 2.63$ for calm conditions ($U_{10} \approx 4$ m s^{-1}), and to 2.37 for above average conditions ($U_{10} \approx 7$ m s^{-1}). A similar decrease is observed for the coastal cell: $\alpha = 2.69$ without mixing, decreasing to $\alpha = 2.60$ ($U_{10} \approx 4$ m s^{-1}) and $\alpha = 2.34$ ($U_{10} \approx 7$ m s^{-1}). Similar to the model, a slightly lower α is calculated for the measurements near the coast (2.49 ± 0.06) compared to measurements further away from the coast (2.53 ± 0.04), although this difference is not significant.

Few PSD measurements are available for beaches. Two examples are shown in figure 7(a): one from the Mediterranean (Constant *et al* 2019), and one for which both the NSD and MSD were available (Fok *et al* 2017). The measurements on beaches have much lower power law slopes ($\alpha < 1.60$) compared to measurements in the water. This is also captured by the model, meaning size-selective resuspension indeed seems to play an important role. In the beach cell the modelled power law slope of $\alpha = 2.02$ is higher than the measured ones, which might indicate that size-selective beaching should be taken in account as well.

Figure 7(b) presents the modelled MSDs. Vertical mixing has a large influence on the measured mass for small particle sizes: even under calm conditions, the measured mass for particles of 0.1 mm is almost three orders of magnitude lower than without mixing. Unfortunately, there is very limited observational data reporting MSDs, so the comparison to data is more limited than for the NSDs in figure 7(a). On beaches, the model matches the set of measurement well, but more data are necessary to further verify this. Large fragments are expected to dominate in terms of mass on beaches. In the water, α seems to be approximately zero on average. This would mean that the mass contribution would scale roughly quadratically for an increasing size class k, i.e. large fragments also dominate in terms of mass here.

The environmental box model used to model the PSDs is a useful tool for future mass balance studies. The steady-state with the model settings used for figure 7, gives that about 98% of the mass in the system is on the beach, about 2% in the coastal surface water, and about 0.2% in the surface open ocean. This large fraction of plastics stranding is in good agreement with previous mass balance estimates (Lebreton *et al* 2019). It should be noted that other environmental regions, like the ocean floor, are not included in these numbers as these are part of the sinks in the box model (P_S), which continuously take up more mass over time. Secondary microplastics generation can be estimated: for the same model settings, about 6.5×10^{-5}% of the macroplastic (>5 mm) mass breaks down into microplastics per week, about 2.0×10^{-6}% of microplastics become smaller than 0.1 mm. This is orders of magnitude smaller than the estimated sinks, taking up about 5.0×10^{-2}% of the plastic mass per week. Longevity of plastics can be estimated: taking a sudden stop of new plastics entering the marine environment, it would take about 176 years for 99% of the plastic mass to disappear from the surface water and beaches. This is a much longer time scale than given by the conceptual model in Koelmans *et al* (2017), where for a similar stop of new plastics, almost all plastic mass was removed from the ocean surface layer within three years. Plastic residence times are highly dependent on the input scenarios: in Koelmans *et al* (2017), 3% of the world plastic pollution was estimated to enter the ocean. Here, the input scenario from Kaandorp *et al* (2020) is used for the Mediterranean Sea, where less than 0.1% of plastic waste from coastal population was estimated to enter the marine environment. These differences show the importance of further mass balance studies to constrain this number.

4. Discussion

4.1. Model limitations

We will give a brief overview of the fragmentation model and environmental box model limitations in this section, which can be addressed in future studies.

The fragmentation model presented here only has few parameters (p, f, and D_N), and assumes that the fragmentation process is scale-invariant. One example where the assumption of scale-invariance might not hold is when only the plastic surface layer gets brittle with microcracks (Andrady 2011). This possibly increases the fragmentation rate below a certain length scale, dependent on how far UV radiation penetrates the polymer and the polymer type. It is assumed that f is directly proportional to the time that particles spend on the beach, leading to a constant fragmentation rate λ. In e.g. Charalambous (2015), it was shown that grinding can become less efficient as particles become smaller, which might lead to e.g. a logarithmic relation instead.

One source of uncertainty in the fragmentation model is the fact that parameters are calibrated using experimental data for low-density polyethylene and polypropylene pellets only (Song *et al* 2017). More research is necessary to quantify how fragmentation differs between low-density and high-density polyethylene, and for other polymers found in the environment not taken in account here (e.g. polyamides

and polystyrene, which form a substantial fraction of polymers found in the Mediterranean Sea surface water (Pedrotti *et al* 2016)). PSDs are quite sensitive to the choice of λ (see figure 6) and p (see the supplementary material, section S1), for which the values are still quite uncertain. More experimental data are required to further constrain these parameters and to estimate how they vary globally. Finally, it is still uncertain which processes can extend the degradation process to finer scales than mechanical abrasion, and the magnitude of their influence (e.g. photochemical oxidation (Ward *et al* 2019), or biodegradation (Molitor *et al* 2019, Gerritse *et al* 2020)).

The environmental box model is an idealized section of the marine environment, only considering overall transport between cells representing the open ocean, coastal water, and beach. Regional influences are not taken in account and should be investigated in the future: think, for example, about different types of coasts (Weideman *et al* 2020) with different particle residence times and beaching timescales (Samaras *et al* 2014). A number of assumptions were made to arrive at the environmental box model. We assume that the majority of plastic particles are fragments (Cózar *et al* 2014, Suaria *et al* 2016), which means that the influence of primary plastics such as resin pellets (Turner and Holmes 2011) or plastic beads from consumer products (Fendall and Sewell 2009) is neglected. It is assumed that fragmentation is dominant on beaches (Andrady 2011). Fragmentation in the water column is neglected, which might be for example induced by hydrolysis and biodegradation (Gerritse *et al* 2020), or ingestion and scraping by marine organisms (Reisser *et al* 2014, Mateos-Cárdenas *et al* 2020). It is furthermore assumed that new plastic particles are introduced on the beach. In reality there will be a combination of inputs into the different environmental compartments depending on the sources. In the supplementary material (section S1) it is shown that this assumption has no significant effect on the results. Finally, it is assumed that the rate of plastic removal from the marine environment is constant. Although we are looking at time scales in the order of years here, seasonality might have an effect on the removal rate by influencing, for example, biological activity.

We demonstrated the model capabilities using a set-up based on the Mediterranean Sea. One source of uncertainty is that the resuspension time scale is obtained from Hinata *et al* (2017), based on experiments at a Japanese beach. A sensitivity study for this parameter is given in the supplementary material (section S1). Future studies should look at how this parameter varies for different beaches globally. The size of new plastics introduced into the marine environment is still uncertain: it is fixed to 200 mm here, while in reality this will be a spectrum of different sizes, see the supplementary material (sections S1, S4) for more information.

4.2. Fragmentation models and size distribution data

The cascading fragmentation model by Charalambous (2015) used in this work, shows quite good correspondence with experimental data from Song *et al* (2017) (see figure 5). A benefit of the fragmentation model presented here, is the ability to model the mass size distribution (MSD) as well, which can help us obtain a better understanding of the marine plastic mass budget. MSD data to validate the model is currently lacking however, for example to verify whether the larger size classes indeed make up most of the environmental plastic mass. More PSD data from beaches would allow for better constraining residence times of plastic particles on beaches and in coastal waters, and more data from marine sediment might give insight in the role of size-selective sinking, induced by e.g. biofouling (Kooi *et al* 2017).

Fragmentation models for plastics have been introduced in previous works, such as in Cózar *et al* (2014). They focused mainly on spatial dimensionality: $\alpha = 3$ in the NSD was related to three-dimensional fragmentation, i.e. a cube splitting into 8 smaller cubes. Care should be taken in future studies that when working with logarithmic binning, the normalized NSD (units: n mm^{-1}) slope decreases by one compared to the discrete NSD (units: n), see figure 3. This was overlooked in Cózar *et al* (2014): $\alpha = 3$ would correspond to two-dimensional fragmentation with their model, see the supplementary material (section S5) for further explanation. Normalization is also important to take into account when describing plastic particle size in terms of a probability density function (Kooi and Koelmans 2019), specifying the probability per unit length (units: mm^{-1}). Finally, estimating α is not trivial: fitting straight lines on log-log transformed data induces large biases, maximum likelihood approaches are more suitable, see e.g. Newman (2005) and Virkar and Clauset (2014).

5. Conclusions

In this work, we modelled particle size distributions (PSDs) of plastics in the marine environment, by considering a cascading fragmentation model, and a box model taking in account size-selective transport between the open ocean, coastal water, and beach. We showed that the cascading fragmentation model is able to explain the power law observed in PSDs from the environment and experimental fragmentation studies, that size-selective transport plays an important role near the coast, and that vertical mixing in the water column has a strong impact on measured PSDs.

Understanding the nature of PSDs and how they differ in environmental regions can help us get a better understanding of the marine plastic mass budget. Previous conceptual mass balance studies, such as the ones by Koelmans *et al* (2017) and Lebreton *et al* (2019), did consider fragmentation, but only for 2 or 3 categories (macro-, micro- and nanoplastics). Here, we model a range of size classes. This way, we can not only predict which environmental compartment contains most plastic mass, but also which size ranges.

We applied the combined fragmentation and environmental box model to a scenario based on the Mediterranean Sea. For the steady-state, we estimate that of buoyant plastics about 98% of plastics reside on beaches, about 2% in coastal surface waters, and about 0.2% in the surface open ocean. On one hand, the model predicts fragmentation to play an important role in terms of generating a large number of plastic fragments. On the other hand, fragmentation seems to play a minor role in the mass budget compared to other environmental sinks, by moving mass from large to small particle size classes.

Overall, the idealized model presented here is a valuable tool to efficiently test hypotheses regarding the marine plastic mass budget. It can be checked whether a certain hypothesis leads to results which are consistent with current knowledge of plastic sources, sinks, transport, fragmentation, and observational data of plastic concentrations and PSDs. At a later stage, the fragmentation model could also be applied to more complex physical models, taking into account spatial and temporal variability of plastic transport in the marine environment.

Data availability statement

The data that support the findings of this study are openly available at the following URL/DOI: https://github.com/OceanParcels/ContinuousCascadingFragmentation.

Acknowledgments

This work was supported through funding from the European Research Council (ERC) under the European Union Horizon 2020 research and innovation programme (Grant Agreement No. 715386). This work was carried out on the Dutch national e-infrastructure with the support of SURF Cooperative (Project No. 16371). We would like to thank Dr Wonjoon Shim and Dr Young Kyoung Song for their data on plastic fragmentation, Dr Marie Poulain-Zarcos for providing data on particle sizes and vertical mixing, Dr Andrés Cózar and Dr Atsuhiko Isobe for providing raw particle size distribution data. We would like to acknowledge the two anonymous reviewers of this manuscript, whose thoughtful comments substantially improved the clarity and readability of this work.

ORCID iDs

Mikael L A Kaandorp https://orcid.org/0000-0003-3744-6789
Henk A Dijkstra https://orcid.org/0000-0001-5817-7675
Erik van Sebille https://orcid.org/0000-0003-2041-0703

References

Abeynayaka A, Kojima F, Miwa Y, Ito N, Nihei Y, Fukunaga Y, Yashima Y and Itsubo N 2020 Rapid sampling of suspended and floating microplastics in challenging riverine and coastal water environments in Japan *Water* **12** 1903

Andrady A L 2011 Microplastics in the marine environment *Mar. Pollut. Bull.* **62** 1596–605

Andrady A L, Pegram J E and Song Y 1993 Studies on enhanced degradable plastics. II. Weathering of enhanced photodegradable polyethylenes under marine and freshwater floating exposure *J. Environ. Polym. Degrad.* **1** 117–26

Bird N R A, Tarquis A M and Whitmore A P 2009 Modeling dynamic fragmentation of soil *Vadose Zone J.* **8** 197–201

Breivik Ø, Bidlot J R and Janssen P A E M 2016 A Stokes drift approximation based on the Phillips spectrum *Ocean Model.* **100** 49–56

Charalambous C 2015 On the evolution of particle fragmentation with applications to planetary surfaces *PhD Thesis* Imperial College, London

Chor T, Yang Di, Meneveau C and Chamecki M 2018 A turbulence velocity scale for predicting the fate of Buoyant materials in the oceanic mixed layer *Geophys. Res. Lett.* **45** 11817–26

Constant M, Kerhervé P, Mino-Vercellio-Verollet M, Dumontier M, Vidal A Sànchez, Canals M and Heussner S 2019 Beached microplastics in the Northwestern Mediterranean Sea *Mar. Pollut. Bull.* **142** 263–73

Cózar A *et al* 2014 Plastic debris in the open ocean *Proc. Natl Acad. Sci. USA* **111** 10239–44

Cózar A, Sanz-Martín M, Martı E, Ubeda B, Gálvez J A, Irigoien X and Duarte C M 2015 Plastic accumulation in the mediterranean sea *PLoS One* **10** 1–12

Delandmeter P and van Sebille E 2019 The Parcels v2. 0 Lagrangian framework: new field interpolation schemes *Geosci. Model Dev.* **12** 3571–84

Efimova I, Bagaeva M, Bagaev A, Kileso A and Chubarenko I P 2018 Secondary microplastics generation in the sea swash zone with coarse bottom sediments: laboratory experiments *Frontiers Mar. Sci.* **5** 313

Enders K, Lenz R, Stedmon C A and Nielsen T G 2015 Abundance, size and polymer composition of marine microplastics > 10 μm in the Atlantic Ocean and their modelled vertical distribution *Mar. Pollut. Bull.* **100** 70–81

Erni-Cassola G, Gibson M I, Thompson R C and Christie-Oleza J A 2017 Lost, but found with Nile red: a novel method for detecting and quantifying small microplastics (1 mm to 20 μm) in environmental samples *Environ. Sci. Technol.* **51** 13641–8

Fazey F M C and Ryan P G 2016 Biofouling on buoyant marine plastics: an experimental study into the effect of size on surface longevity *Environ. Pollut.* **210** 354–60

Fendall L S and Sewell M A 2009 Contributing to marine pollution by washing your face: microplastics in facial cleansers *Mar. Pollut. Bull.* **58** 1225–8

Fok L, Cheung P K, Tang G and Li W C 2017 Size distribution of stranded small plastic debris on the coast of Guangdong, South China *Environ. Pollut.* **220** 407–12

Gerritse J, Leslie H A, de Tender C A, Devriese L I and Vethaak A D 2020 Fragmentation of plastic objects in a laboratory seawater microcosm *Sci. Rep.* **10** 1–16

Gregory A S, Bird N R A, Watts C W and Whitmore A P 2012 An assessment of a new model of dynamic fragmentation of soil with test data *Soil Tillage Res.* **120** 61–8
Herman J R, Krotkov N, Celarier E, Larko D and Labow G 1999 Distribution of UV radiation at the Earth's surface from TOMS-measured UV-backscattered radiances *J. Geophys. Res.* **104** 12059–76
Hersbach H *et al* 2020 The ERA5 global reanalysis *Q. J. R. Meteorol. Soc.* **146** 1999–2049
Hinata H, Mori K, Ohno K, Miyao Y and Kataoka T 2017 An estimation of the average residence times and onshore-offshore diffusivities of beached microplastics based on the population decay of tagged meso- and macrolitter *Mar. Pollut. Bull.* **122** 17–26
Hinata H, Sagawa N, Kataoka T and Takeoka H 2020 Numerical modeling of the beach process of marine plastics: a probabilistic and diagnostic approach with a particle tracking method *Mar. Pollut. Bull.* **152** 110910
Isobe A, Kubo K, Tamura Y, Nakashima E and Fujii N 2014 Selective transport of microplastics and mesoplastics by drifting in coastal waters *Mar. Pollut. Bull.* **89** 324–30
Isobe A, Uchida K, Tokai T and Iwasaki S 2015 East Asian seas: a hot spot of pelagic microplastics East Asian seas: a hot spot of pelagic microplastics *Mar. Pollut. Bull.* **101** 618–23
Iwasaki S, Isobe A, Kako S, Uchida K and Tokai T 2017 Fate of microplastics and mesoplastics carried by surface currents and wind waves: a numerical model approach in the Sea of Japan *Mar. Pollut. Bull.* **121** 85–96
Jambeck J R, Geyer R, Wilcox C, Siegler T R, Perryman M, Andrady A, Narayan R and Law K L 2015 Plastic waste inputs from land into the ocean *Science* **347** 768–71
Jansen M, van Velzen U T and Pretz T 2015 *Handbook for Sorting of Plastic Packaging Waste Concentrates* (Wageningen: Wageningen UR—Food and Biobased Research)
Kaandorp M L A, Dijkstra H A and van Sebille E 2020 Closing the Mediterranean marine floating plastic mass budget: inverse modelling of sources and sinks *Environ. Sci. Technol.* **54** 11980–9
Kalogerakis N, Karkanorachaki K, Kalogerakis G C, Triantafyllidi E I, Gotsis A D, Partsinevelos P and Fava F 2017 Microplastics generation: onset of fragmentation of polyethylene films in marine environment mesocosms *Frontiers Mar. Sci.* **4** 84
Koelmans A A, Kooi M, Law K L and van Sebille E 2017 All is not lost: deriving a top-down mass budget of plastic at sea *Environ. Res. Lett.* **12** 114028
Kooi M and Koelmans A A 2019 Simplifying microplastic via continuous probability distributions for size, shape and density *Environ. Sci. Technol. Lett.* **6** 551–7
Kooi M, van Nes E H, Scheffer M and Koelmans A A 2017 Ups and downs in the ocean: effects of biofouling on vertical transport of microplastics *Environ. Sci. Technol.* **51** 7963–71
Kukulka T, Proskurowski G, Morét-Ferguson S, Meyer D W and Law K L 2012 The effect of wind mixing on the vertical distribution of buoyant plastic debris *Geophys. Res. Lett.* **39** 1–6
Lebreton L, Egger M and Slat B 2019 A global mass budget for positively buoyant macroplastic debris in the ocean *Sci. Rep.* **9** 12922
Liubartseva S, Coppini G, Lecci R and Clementi E 2018 Tracking plastics in the Mediterranean: 2D Lagrangian model *Mar. Pollut. Bull.* **129** 151–62
Mateos-Cárdenas A, O'Halloran J, van Pelt F N A M and Jansen M A K 2020 Rapid fragmentation of microplastics by the freshwater amphipod Gammarus duebeni (Lillj.) *Sci. Rep.* **10** 1–12
Menna M, Gerin R, Bussani A and Poulain P-M 2017 The OGS Mediterranean Drifter Dataset: 1986–2016 *Technical Report*
Molitor R, Bollinger A, Kubicki S, Loeschcke A, Jaeger K E and Thies S 2019 Agar plate-based screening methods for the identification of polyester hydrolysis by Pseudomonas species *Microbial Biotechnol.* **13** 274–84
Newman M E J 2005 Power laws, Pareto distributions and Zipf's law *Contemp. Phys.* **46** 323–51
Onink V, Wichmann D, Delandmeter P and van Sebille E 2019 The role of Ekman currents, geostrophy and stokes drift in the accumulation of floating microplastic *J. Geophys. Res.: Oceans* **124** 1474–90
Pedrotti M L, Petit S, Elineau A, Bruzaud S, Crebassa J C, Dumontet B, Martí E, Gorsky G and Cózar Aes 2016 Changes in the floating plastic pollution of the Mediterranean sea in relation to the distance to land *PLoS One* **11** 1–14
Poulain M, Mercier M J, Brach L, Martignac M, Routaboul C, Perez E, Desjean M C and Halle A 2019 Small microplastics as a main contributor to plastic mass balance in the North Atlantic Subtropical Gyre *Environ. Sci. Technol.* **53** 1157–64
Reisser J, Shaw J, Hallegraeff G, Proietti M, Barnes D K A, Thums M, Wilcox C, Hardesty B D and Pattiaratchi C 2014 Millimeter-sized marine plastics: a new pelagic habitat for microorganisms and invertebrates *PLoS One* **9** 1–11
Reisser J, Slat B, Noble K, Du Plessis K, Epp M, Proietti M, De Sonneville J, Becker T and Pattiaratchi C 2015 The vertical distribution of buoyant plastics at sea: an observational study in the North Atlantic Gyre *Biogeosciences* **12** 1249–56
Ruiz-Orejón L F, Sardá R and Ramis-Pujol J 2018 Now, you see me: high concentrations of floating plastic debris in the coastal waters of the Balearic Islands (Spain) *Mar. Pollut. Bull.* **133** 636–46
Ryan P G 2015 Does size and buoyancy affect the long-distance transport of floating debris? *Environ. Res. Lett.* **10** 84019
Samaras A G, De Dominicis M, Archetti R, Lamberti A, and Pinardi N 2014 Towards improving the representation of beaching in oil spill models: a case study *Mar. Pollut. Bull.* **88** 91–101
Song Y K, Hong S H, Jang Mi, Han G M, Jung S W and Shim W J 2017 Combined effects of UV exposure duration and mechanical abrasion on microplastic fragmentation by polymer type *Environ. Sci. Technol.* **51** 4368–76
Suaria G, Avio C G, Mineo A, Lattin G L, Magaldi M G, Belmonte G, Moore C J, Regoli F and Aliani S 2016 The Mediterranean plastic soup synthetic polymers in Mediterranean surface waters *Sci. Rep.* **6** 1–10
Tokai T, Uchida K, Kuroda M and Isobe A 2021 Mesh selectivity of neuston nets for microplastics *Mar. Pollut. Bull.* **165** 112111
Turcotte D L 1986 Fractals and fragmentation *J. Geophys. Res.* **91** 1921–6
Turner A and Holmes L 2011 Occurrence, distribution and characteristics of beached plastic production pellets on the island of Malta (central Mediterranean) *Mar. Pollut. Bull.* **62** 377–81
van Sebille E *et al* 2020 The physical oceanography of the transport of floating marine debris *Environ. Res. Lett.* **15** 023003
Virkar Y and Clauset A 2014 Power-law distributions in binned empirical data *Ann. Appl. Stat.* **8** 89–119
van den Bremer T S and Breivik Ø 2017 Stokes Drift Phil. Trans. R. Soc. A. **376** 20170104
Ward C P, Armstrong C J, Walsh A N, Jackson J H and Reddy C M 2019 Sunlight converts polystyrene to carbon dioxide and dissolved organic carbon *Environ. Sci. Technol. Lett.* **6** 669–74
Weideman E A, Perold V, Omardien A, Smyth L K and Ryan P G 2020 Quantifying temporal trends in anthropogenic litter in a rocky intertidal habitat *Mar. Pollut. Bull.* **160** 111543